

UPSCALED GEOCELLULAR FLOW MODEL OF POTENTIAL ACROSS- AND ALONG-FAULT LEAKAGE USING SHALE GOUGE RATIO.

T.I. Bjørnarå^{1*}, E.M. Haines², E. Skurtveit^{1,2}

¹ NGI, Oslo, Norway, ² University of Oslo, Norway

* Corresponding author e-mail: tore.ingvald.bjornara@ngi.no

Abstract

Every CCS project has an inherent risk of leakage. Faults are difficult to characterize because they are structurally complex and limited subsurface field-data is typically available; hence the properties need to be inferred elsewhere, e.g. well-logs and seismic. For example, the shale gouge ratio (SGR) is typically used today in the oil and gas exploration to estimate sealing properties of faults, by utilizing VShale well logs.

Here we extend the methodology to account for along-fault flow where the complex structural composition of a fault is conceptually described by a geocellular model that is stochastically constructed using modelled SGR from a real fault (Vette Fault) in the Horda platform, North Sea, offshore Norway. A detailed geocellular fault model can be extremely computationally expensive, therefore an upscaled formulation is defined and validated. This formulation also extends the applicability of a multi-layered geocellular model by allowing slip-surface(s) to be a natural component of the fault core. The validation model is applied to a single-phase fluid flow problem, simulating fluid migration from a pressurized reservoir and across and up along a fault that intersects the reservoir; a scenario directly relevant to CO₂ storage where the fault is (temporary) outside the reach of the injected CO₂ plume.

The presented upscaled formulation of a multi-layered geocellular model was found to have a high and consistent accuracy, relative to a full-dimensional reference model, with generally less than 4 % error (or less than 8 % within 95 % confidence interval) in calculated along- and across-fault flow. The focus here is on proof of concept and validation of a generic upscaled multi-layered geocellular model, but some general observations can be made. For across-fault flow, an increase in variability in fault composition resulted in a reduced flow-rate and less spread in flow-rate. For along-fault flow, increasing variability in fault composition had little effect on mean flow-rate, but resulted in smaller spread.

Keywords: CO₂ storage, across- and along-fault flow, Shale Gouge Ratio (SGR), fault leakage

1. Introduction

Recently, the Norwegian government launched Longship, a first project for full-scale Carbon Capture and Storage (CCS) in Norway. The Aurora storage site in the Norwegian Horda Platform area is currently under development of CO₂ injection, but the area also has large potential for upscaling the storage volumes. The Smeaheia fault block, located between the Troll gas field and the Norway west coast has shown promising storage potential within the Sognefjord Formation, bounded by two regional fault systems, the Vette Fault Zone (VFZ) and the Øygarden fault complex (ØFC), in the west and east, respectively, see Figure 1. The future success of this faulted block as offshore CO₂ storage is highly dependent on maturing the geological understanding and fault seal potential of the area (Mulrooney et al., 2020, Wu et al., 2021).

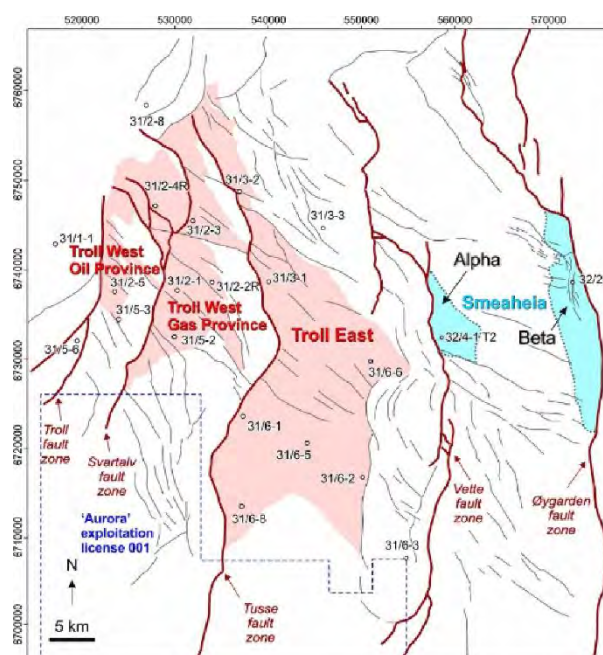


Figure 1: Structural map of the Troll field area (Wu et al., 2019). The Smeaheia-site is shown with two storage prospects (Alpha and Beta) bounded laterally to the west and east by the Vette Fault (VF) and Øygarden Fault (ØGF), respectively.

The challenge with CO₂ storage is to ensure its integrity against leakage of injected CO₂. Three potential leakage pathways for CO₂ are: (i) migration and diffusions through intact caprock, (ii) migration by fracturing of the caprock and (iii) migration along pre-existing fractures and faults (Niemi et al., 2017). Besides (iv) leakage up wellbores, (iii) is potentially the most critical mechanism and most difficult to characterize in terms of leakage risk. Faults can have both sealing or conductive properties, making them complex geological structures that can both limit the storage capacity and be detrimental to the storage integrity.

There is a general need for improved understanding of fluid flow in faults, particularly for large regional-scale faults. The geometry may be constrained by seismic and missing fault attributes can be approximated using correlations, e.g. Torabi & Berg (2011). However, the main challenge is to characterize hydraulic properties of faults from available data. One of the aspects that makes large faults complex is the unknown variability and distribution of associated fault rocks (gouge, breccia, cataclasite, mylonite, etc.) within the fault core (Grant, 2020), and the resulting hydraulic properties.

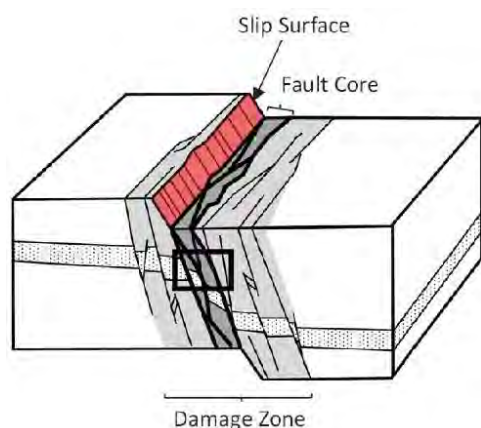


Figure 2: Illustration of a typical fault architecture, as originally defined by Caine et al. (1996) (figure from Grant 2020, originally modified from Torabi & Berg, 2011).

The two most common representations and/or conceptualizations of faults and its hydraulic structure are the single- and two-component description of a fault, see Figure 2 and Figure 3. In the single-component model, the fault zone (FZ) is homogenized to an isotropic or anisotropic permeability structure with principal permeabilities in the across- and along-fault directions. In the two-component fault model, the fault zone is divided into a fault core (FC) surrounded by a damage zone (DZ). This latter model was further characterized by Caine et al. (1996) by distinguishing the fraction of FC width and DZ width relative to the total FZ width and recognizing that, in general, the FC promotes sealing (barrier) properties while the DZ promotes conductive (conduit) properties. Fault classification by Caine et al. (1996) is based on geometric properties of FC and DZ, but other modified two-component fault classifications have been proposed, e.g. by Matonti et al. (2012) which is based on fracturation, p -wave velocity and porosity.

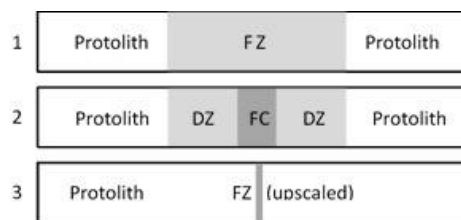


Figure 3: Typical conceptualizations of faults found in the literature. (1) Single-component model of a fault zone (FZ). (2) Two-component model where the fault zone is divided into a fault core (FC) surrounded by a damage zone (DZ). (3) Upscaled/dimensionally reduced version of single- and/or two-component fault model where the FZ, or FC and DZ, is mathematically described as a surface in 3D, or a line in 2D, with virtual thicknesses.

Another way to distinguish the fault properties is to divide the FZ into a zone of low- and high-strain, or displacement. The high-strain zone corresponds to the fault core with the largest deformations and where the fault rock is developed. The low-strain zone corresponds to the damage zone. The host rock material, before faulting, decides what properties the strain-zones will have after faulting. This conceptualization has resulted in several mixing models, or clay smear models, where sequences of alternating sandstone and shales are displaced by faults: shale smear factor model (SSF, Lindsay et al., 1993), clay smear potential model (CSP, Lehner and Pilaar, 1997), shale gouge ratio model (SGR, Yielding et al., 1997) and extensions of these.

SGR is a measure of the net shale/clay content at a location along the slip direction of a fault. It has been shown that the clay-content typically has an exponential influence on the fault core permeability, and there are several correlations between fault core permeability and SGR, e.g. Sperrevik et al. (2012), and Childs et al. (2007). Further, a relationship has been defined between the predicted SGR and measured column heights (Yielding et al., 2010). Hence, SGR is commonly used to predict the sealing potential of a fault and its ability to contain a maximum hydrocarbon column.

There have been several attempts in advancing the characterization of hydraulic properties of faults. The single- and two-component models illustrated in Figure 3 are not adequate because an average model cannot capture the variability, across and along the fault, and therefore may not capture potential spill-points along a seemingly sufficiently tight caprock. This has led to the development of geocellular fault models, where the fault core is approximated by geocells and the geocell properties are populated stochastically, e.g. fault rock facies (Fault Facies Project at the University of Bergen, e.g. Fredman et al., 2007, Kolyukhin & Tveranger, 2015, and references therein) or upscaled SGR from seismic and well-logs (Manzocchi et al., 1999). This is done by converting the locally upscaled SGR-value to a permeability, which is then used to calculate a transmissibility multiplier for across-fault flow characterization that can be used in reservoir-scale models (Manzocchi et al., 1999).

An important component of a fault is the slip-surface(s) in the high-strain FC. The slip-surface(s) of a fault can be straight or undulating (anastomosing), they can occur

single or in an arrangement, e.g. en echelon. A distinct feature of a slip-surface is that it has an extremely large aspect ratio and is therefore missing in geocellular models. However, slip-surface(s) can be an important factor when considering activation of a fault and the dynamic changes in its sealing properties. Slip-surfaces, like discrete fractures, are almost always defined as a dimensional reduced object with a virtual thickness.

Here we present a model that combines the fault variability of the geocellular model with the inclusion of slip-surface(s) in the fault. We use the geocellular approach to characterize fluid flow both across and along a regional-scale fault. Then we formulate the geocellular fault using upscaled equations for single-phase fluid flow. The upscaled multi-layer geocellular model is validated by solution-comparison with a model using the full-dimensional formulation. The strength of the upscaled formulation of a geocellular fault is that it uses an already applied methodology based on SGR (hence, also transmissibility multiplier), and the upscaled formulation is identical to a dimensionally reduced slip-surface and can therefore easily be added as an integral part of the fault description. Also, the less complex and numerically efficient upscaled formulation opens the possibility to do a wide range of investigations and what-if analyses related to faults, both in 2D and 3D, and some preliminary analysis are also presented.

2. Model and method

The focus in this manuscript is on the validation of an upscaled geocellular model, and in particular the across- and along-fault fluid flow and flow rates out of storage reservoir. Hence, the material properties of surrounding formations, including the reservoir, are generic and therefore not discussed in detail. This simplification also applies to the geometry, e.g. we do not consider the displacement (throw) of the fault and therefore the host rocks on opposite sides of the fault are not shifted relative to each other.

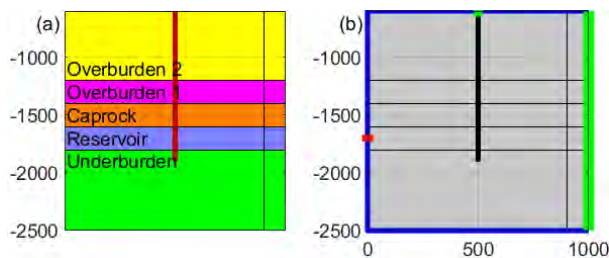


Figure 4: Geometry of validation model with the various lithologies indicated. The total height of the model is 1900 m (from -2500 m to -600 m). The total width of the model is 10 km. (a) The various formations in the model. The fault core (FC), indicated by the red vertical line, is 15 m thick and located app. 500 m from the left boundary. In the full-dimensional model the fault is defined by a domain, and in the upscaled model the fault is defined by a zero-thickness line (internal boundary in the model). (b) Boundary conditions: Inlet (pressure, red), no-flow (blue) and outlet (reference pressure, green).

The scenario that is treated here is a pressurized reservoir, e.g. due to injection of CO₂. The reservoir is intersected

by, and hydraulically connected to, a vertical fault that extends up to the top of the overburden, at -600 m bmsl, see geometry in Figure 4. Although the scenario presented here is related to CO₂ storage, the fault is assumed, for simplicity, to be outside the reach of the CO₂ plume and is therefore a single-phase fluid flow problem.

The complex structural composition of the FC is conceptually described by a geocellular model. The cells, stochastically constructed, have a randomly generated height between 10-100 m. The geocells allow for variability in the permeability structure, which can be populated stochastically from either fault facies (e.g. Wilson et al., 2020, Grant, 2020) or SGR (Yielding et al., 1997). Here we use a vertical cross-section (red line in Figure 5, center) of a 3D model of the SGR for a real fault on the Horda platform in the North Sea (Vette Fault, see Figure 1, a 2 km wide section is shown in Figure 5, left) as basis for the considered scenario. The vertical cross-section is the mean SGR-profile and using a normal probability distribution function with a standard deviation of 14 % (derived from Foxford et al., 1998; Freeman et al., 2008), the geocellular fault is populated. In Figure 5 (right) a geocellular fault (core) with 8 parallel layers is shown, the grey dots indicate the corresponding statistical spread in SGR-values along the vertical profile (each grey dot represents a geocell).

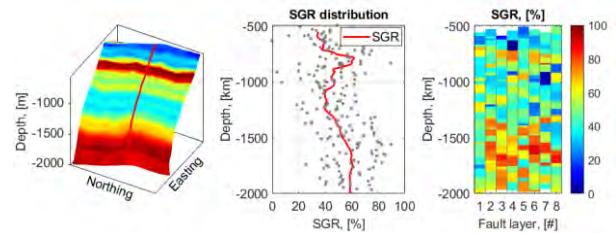


Figure 5: Left: A 2 km wide section of SGR (%) along the Vette fault (cold blue to hot red represents SGR-values of 28-62 %, respectively). Center: Red line is the average SGR-profile shown in left panel. Right: Example of a geocellular model of SGR. The SGR-values in the geocells are shown by the grey dots in the center figure.

2.1 Numerical model

The numerical model is a reservoir-scale model with a geometry as schematically shown in Figure 4. The fluid flow is described by the mass conservation equation for the fluid combined with Darcy's law for the volumetric flux rate \mathbf{q} [m/s]:

$$S\rho\frac{\partial p}{\partial t} + \nabla \cdot (\rho\mathbf{q}) = 0, \mathbf{q} = -\frac{k}{\mu}(\nabla p - \rho\mathbf{g}) \quad \text{Eq. 1}$$

where ρ [kg/m³] is the fluid density, k [m²] is the permeability, μ [Pa·s] is the fluid viscosity, \mathbf{g} [m/s²] is the gravity vector and where the storage coefficient S [1/Pa] is defined by:

$$S = \frac{b - \phi}{K_s} + \frac{\phi}{K_f} + \frac{b^2}{\lambda + 2G} \quad \text{Eq. 2}$$

where b [-] is the Biot's coefficient, ϕ [-] is the porosity, K_s [Pa] is the bulk modulus of the solid grains, K_f [Pa] is the inverse of the fluid compressibility and λ [Pa] and

G [Pa] Lamé coefficients that are the bulk elastic moduli for the formations. Note that the permeability is isotropic but heterogeneous inside the fault (core), $k = k(x, y)$, and homogeneous in the surrounding formations.

The boundary conditions are illustrated with the geometry in Figure 4 (right). The inlet is a pressure condition: $p_{in} = p_0 + \Delta p$, where p_0 [Pa] is the initial pore pressure and Δp is the pressure increase (due to CO₂ injection in the scenario defined here). The blue boundaries have no-flow condition and the green boundaries are open boundaries with a fixed pressure: $p = p_0$. Note that the boundary conditions here are constructed so that flow can only exit the model either through the top boundary of the fault or on the opposite side of the inlet to better compare the along- and across-fault flow behavior in the upscaled model with the full-dimensional model.

2.2 Upscaled fault flow

The upscaled formulations for fluid flow are particularly useful when modelling structures with high aspect ratio, e.g. slip-surfaces and layers of geocells (as shown in Figure 5, right). The fluid flow in a fault can be composed of two main flow contributions; along-fault flow and across-fault flow. The along-fault flow can be described as tangential flow along the upscaled fault while the across-fault flow can be described as a balance of the fluid flux normal to the upscaled fault that corresponds to the fluid exchange to the surrounding protolith and/or neighboring fault component(s), see illustration in Figure 6.

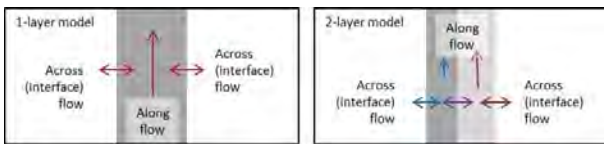


Figure 6: Flow characteristics used in an upscaled model. Left: Single-layer fault model of a fault zone (FZ). Right: Two-layer model of a fault. In a multi-layered (≥ 2 layers) FZ can be further discretized into fault core FC and damage zone(s) DZ.

The tangential fluid flow formulation can be found by integrating the mass conservation equations for the fluid phase across the thickness w_n [m] of a fault layer or component. When assuming that the properties in the fault layer/component are constant, as well as the Darcy-flux, the upscaled (tangential) form of the fluid-flow equations can be expressed as:

$$w_n \left[S_n \rho \frac{\partial p}{\partial t} \nabla_t \cdot (\rho \mathbf{q}_t) \right] = \mathbf{q}_{\Delta, n} \quad \text{Eq. 3}$$

where we have included the fault layer index n and the subscript t indicates tangential component. The Darcy-flux in Eq. 3 is now expressed as:

$$\mathbf{q}_t = -\frac{k_n}{\mu} (\nabla_t p - \rho \mathbf{g}) \quad \text{Eq. 4}$$

The source-term on the right side, $\mathbf{q}_{\Delta, n}$ [kg/m²/s], comes directly from the integration procedure and describes the fluid exchange with the surrounding protolith and/or neighboring fault component(s): across-fault flow.

In the case of no fluid exchange, e.g. if the surrounding protolith and/or neighboring fault component(s) are impermeable, or in the case of continuity in pore pressure, we have that $\mathbf{q}_{\Delta, n} = 0$. However, here we are describing a pore pressure discontinuity and therefore need to describe the fluid exchange. The across-fault flow can be described using a thin-layer approximation of the fluid flux (conceptually similar to Nernst diffusion layer approximation). Flux across an interface, over a distance δ [m] can be expressed as:

$$q = -\rho \frac{\bar{k} \Delta p + \rho g n_z}{\mu \delta} \quad \text{Eq. 5}$$

Here n_z [-] is the vertical component of the normal vector, \bar{k} is the average (harmonic mean) permeability of the domains on both sides of the interface:

$$\bar{k} = \frac{\sum(w_i)}{\sum(w_i/k_i)} \quad \text{Eq. 6}$$

The interface thickness is approximated as:

$$\delta = \sum(w_i) \quad \text{Eq. 7}$$

As mentioned, an advantage with the upscaled formulation is that it is easily extendable (into n -layers) and a layer can, by using the same mathematical formulation, describe flow in a fracture/slip-surface. Eq. 3 and Eq. 4 are the same equations used when modelling fluid flow in a fracture by redefining the porous media permeability k_n to the fracture flow permeability k_f [m²]:

$$k_f = \frac{w_i^2}{12f} \quad \text{Eq. 8}$$

where w_n is now equivalent to the fracture aperture and f [-] is the roughness/friction coefficient. The fracture transmissivity becomes $T_i = w_i^3/(12f)$.

2.3 Model validation

To validate the upscaled formulation of the geocellular fault, a model with a full-dimensional geocellular fault is compared to a model with an upscaled geocellular fault description. The geocells are populated based on SGR, but for simplicity, here only for the permeability. The other material properties vary between the layers according to Table 1.

There are many correlations in the literature that relates SGR and fault permeability (typically the core; FC) and they should be considered site-specific. These correlations are typically exponentially decaying with shale/clay content (e.g. Childs et al., 2002). Here we define such a correlation (for FC) that is linear in SGR and with two end-member permeabilities representing the pure components:

$$\log(k_n) = \text{SGR}_n \cdot \log\left(\frac{k_c}{k_s}\right) + \log(k_s) \quad \text{Eq. 9}$$

where k_c [m²] and k_s [m²] are the permeability of the shale (clay-rich component) and the sandstone, respectively. Here we use that $k_c = 1 \mu\text{D}$ and $k_s = 1 \text{D}$. An alternative correlation for FC is given by Manzocchi et al. (1999):

$$\log(k_n) = 0.4 - 4SGR - \frac{1}{4}\log(D) (1 - SGR)^5 \quad \text{Eq. 10}$$

where D [m] is the fault throw (here we use that $D = 10$ m). These correlations are compared in Figure 7.

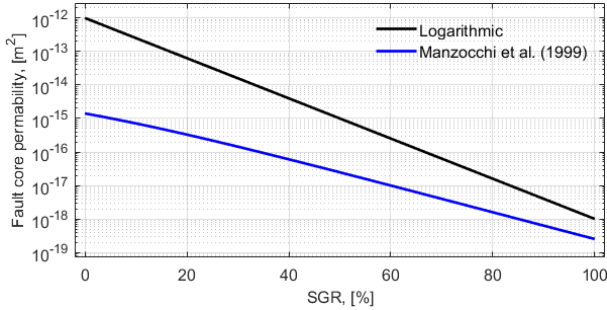


Figure 7: Correlation between SGR and permeability of the fault core from Eq. 9 and Eq. 10.

In this validation we use the correlation in Eq. 9 and it was chosen, over the correlation by Manzocchi et al., (1999), for the purpose of validation of a mathematical model because it gives more (measurable) flow up along and across the fault (has a higher permeability).

The hydro-mechanical properties of the various formations are given in Table 2. Again, note that the values are generic.

Table 1: Hydro-mechanical properties of the fault layers.

Fault layer, [#]	1	2	3	4	5	6	7	8
Perm. k , [m ²]	Varying, based on SGR (Eq. 9)							
Porosity, ϕ , [-]	0.1	0.2	0.3	0.1	0.1	0.2	0.3	0.1
Young's modulus, E , [GPa]	1	2	3	1	2	1	2	3
Poisson's ratio, ν , [-]	0.2	0.3	0.4	0.3	0.2	0.3	0.4	0.3
Biot's coeff. b , [-]	0.9							

Table 2: Hydro-mechanical properties of the formations.

Formation	Underburden	Reservoir	Caprock	Overburden 1	Overburden 2
Permeability, k , [mD]	0.1	1000	0.1	10	1
Porosity, ϕ , [-]	0.1	0.2	0.3	0.1	0.1
Young's mod., E , [GPa]	1	2	3	1	2
Poisson's ratio, ν , [-]	0.2	0.3	0.4	0.3	0.2
Biot's coeff., b [-]	0.9				

3. Results and discussion

In this section we present and discuss the results of the validation model and make some preliminary observations on fluid flow across and along a fault given a specific average SGR profile.

3.1 Validation model

To compare a model with a full-dimensional geocellular fault (full-dimensional model, FM) to a model with an upscaled geocellular fault description (upscaled model, UM), four cases are defined. In all cases, the fault is 15 m thick, but the number of layers in the geocellular description varies: 1, 2, 4, and 8 layers, respectively. Note that in a multi-layered model (2 layers or more), the geocellular layers can describe DZ and FC. However, in this study we do not make that distinction. The fault width is one of the fault attributes that are correlated to other attributes such as length, throw, etc. The value used here is in the higher range of such correlations, see e.g. Torabi & Berg (2011). Considering Figure 5 (right), in case A the vertical profile of the fault is defined using the profile in fault layer 1. For case B, the fault is split into a 2-layered fault where each layer is 7.5 m thick and the vertical profile of the fault layers are defined by fault layer 1 and 2. The same concept is used on case C and case D (4- and 8-layered model, respectively) such that the geocellular SGR-profile for various cases look like Figure 8.

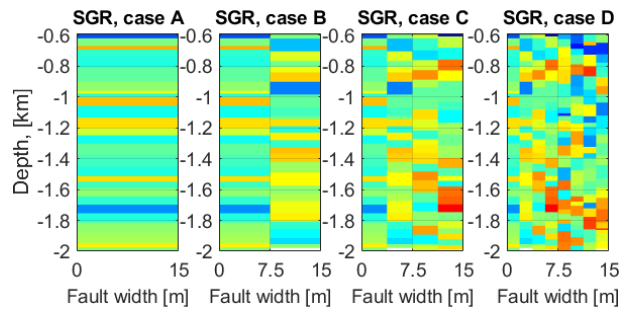


Figure 8: Example of SGR distribution in the fault for the various validation cases. Color-scale is from cold blue to hot red, 0-100 %, respectively.

For every simulation a new randomly generated SGR-"palette" is generated. To validate the UM, a total of 5327 simulations is performed. The mass flow-rate into the reservoir (Q_{in} [kg/s], red boundary in Figure 4) and out of the fault at the top boundary, (Q_{out} [kg/s], green top boundary in Figure 4), were calculated and compared. Note that in the UM the fault at the top boundary is represented by a point. The ratio of the calculated Q_{in} and Q_{out} of the UM versus the FM is shown in Figure 9: $Q_{out,UM}/Q_{out,FM}$ (blue histogram) and $Q_{in,UM}/Q_{in,FM}$ (red histogram). The mode/mean and standard deviation (calculated using Weibull, Wb, and log-logistics, LL, probability distribution functions) are shown in the legends.

The results in Figure 9 shows that the UM (model with upscaled fault) has a tendency of underestimating the flow-rate as the mean values for the ratio between UM and FM are below 1. The more layers in the geocellular

description, the more similar the two models perform, as the mean ratios approach 1.

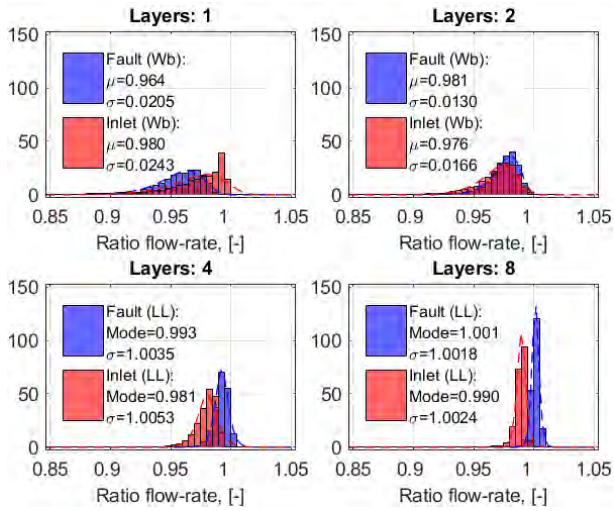


Figure 9: Validation results. Histograms show the ratio of the flow-rate along the fault (blue) and at the inlet (red) between FM and UM for the four cases. Y-axes is probability density estimate (mode/mean and standard deviation: Weibull (Wb) and Log-logistics (LL) probability distribution functions).

The discrepancy between the two models is mainly attributed to the geometrical differences between the models: in the FM the fault has a physical width while in the UM the fault has a virtual thickness, and this impacts the fluid flow tortuosity around the fault. For instance, if the location (boundary) of an SGR-geocell is very close to a formation boundary, there might be situations when it is favorable to by-pass a low-permeable geocell by flowing around it because the flow-path (due to tortuosity) has a lower total resistance to flow. But in general, the UM captures the physical processes related to the upscaled fault with a high accuracy.

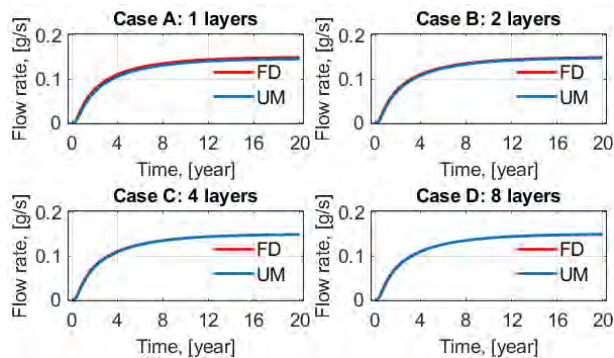


Figure 10: Transient along-fault flow-rate [g/s].

So far, only the steady-state (static) results for the validation model has been shown. To validate the transient solution, we show the comparison for the default average SGR-profile (red curve in Figure 5). The simulation is run for 20 years and the flow rate out of the fault at the top boundary for the two models are compared and shown in Figure 10. The comparison of transient solution is consistent with the comparison of the static solution in Figure 9.

3.2 Preliminary results from a geocellular model

Validation of the UM (upscaled fault model) opens the possibility to many case-studies, including a more thorough analysis of the storage units along the Vette Fault. The model defined so far is generic, with the exception of the chosen SGR-profile, but including the correlation between SGR and the fault permeability. Therefore, here we only include some preliminary results from the validation model.

Note that in the following results we use the inlet flow-rate as a proxy for the across-fault flow-rate. This can be done since the fluid entering the inlet will either exit at the top boundary, by flowing up along the fault, or out the lateral (right) boundary. Some of the fluid may by-pass the fault, by flowing underneath it. However, the permeability in the underburden is low, and combined with a relatively low flow-rate up along the fault, it can be approximated that the flow-rate at the inlet has similar magnitude as the across-fault flow.

The flow-rate at the inlet and up along the fault for the four cases are shown in Figure 11. The flow-rates from the average SGR-profile (not stochastically generated geocells) are shown by the red and blue vertical lines.

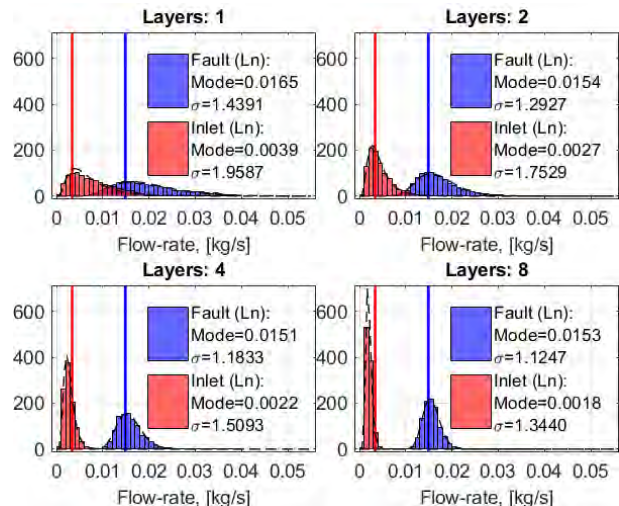


Figure 11: Flow-rate from 1, 2, 4 and 8 layered geocellular models. Note that the along-fault flow-rate is multiplied with a factor 100. The thick vertical lines are the flow-rates calculated using the average SGR-profile across the whole thickness of the fault (fault, blue: 0.0149 kg/s; inlet, red: 0.0034 kg/s). Y-axes is the probability density estimate (mode and standard deviation: Log-normal probability distribution function).

The distribution around the mean value becomes increasingly narrow with increasing number of geocellular layers. This indicates that with increased variability in the composition of the fault the average profile becomes more appropriate to use, particularly for the along-fault flow where the average SGR-profiles match with the mean flow-rates (blue histogram, Figure 11), for all cases considered, see also Figure 12 (left). However, for the across-fault flow (using inlet flow-rate as proxy), using the average SGR-profile seems to overestimate the flow-rate with increasing variability in the fault (increasing number of layers). This is better illustrated in Figure 12: blue and green histogram means

are consistent, while the red and magenta histogram means show a shift towards lower flow-rate with increasing number of geocellular layers.

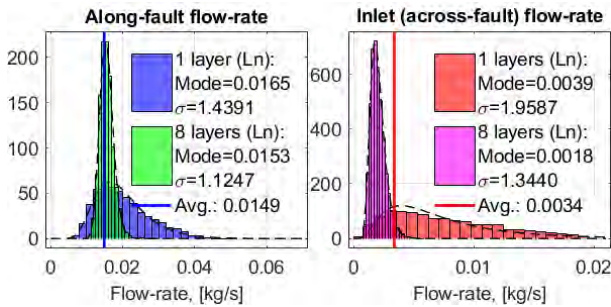


Figure 12: Flow-rate from 1 and 8 layered geocellular models. Note that the along-fault flow-rate (left figure) is multiplied with a factor 100 (for visualization purposes). The thick vertical lines are the flow-rates calculated using the average SGR-profile across the whole thickness of the fault. Y-axes is the probability density estimate (mode and standard deviation: Log-normal probability distribution function).

The flow-rates for a 1-layered geocellular model is compared to flow rates for 2-, 4- and 8-layered models in Figure 13.

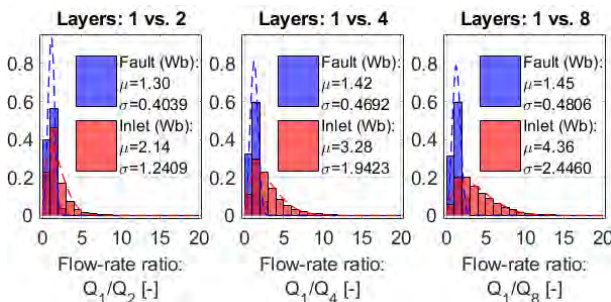


Figure 13: Ratio of flow-rate along-fault (blue) and across-fault (red) for a single layered geocellular model (Q_1) versus 2-, 4- and 8-layered geocellular model; Q_2 , Q_4 and Q_8 . Y-axes is the probability density estimate (mean and standard deviation: Weibull probability distribution function).

In Figure 14 we show the ratio of the along-fault to the across-fault flow-rate.

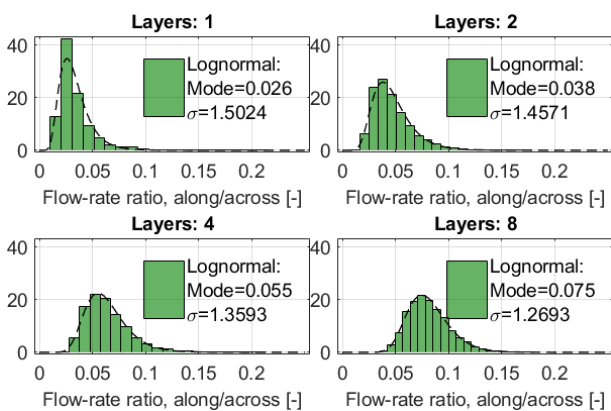


Figure 14: Ratio of flow-rate for along-fault vs. across-fault, y-axes is the probability density estimate (mode and standard deviation: Log-normal probability distribution function).

The comparison in Figure 13 shows that the ratio of the along-fault flow-rate is almost constant and independent of number of layers (ratio around 1.3-1.45, blue histograms). However, the spread in the ratio for across-

fault flow-rate is increasing with increasing number of layers (red histograms). The increasing spread is because the increasing number of layers makes the possibility of across-fault connectivity more homogeneous. Figure 14 shows the ratio of the along-fault to the across-fault flow-rate. The ratio is increasing by a factor three when going from 1 to 8 layers, indicating that increasing fault variability stimulates less fluid to migrate across-fault (since along-fault flow rate is almost constant, e.g. see Figure 10).

3.3 Implications for CO₂ storage

Since fluid migration along pre-existing fractures and faults is the most likely leakage mechanism for CO₂ storage projects, the methodology shown here can be used in a fault derisking workflow. Also, in the case of a sealing FC, but a conductive DZ (implying that across-fault flow is negligible while along-fault flow can be significant), a multi-layered approach is necessary.

Here the fault can be characterized as an assemblage of components with various permeability. However, capillary threshold pressure can also be estimated from clay content, hence leakage of CO₂ is not only relying on favorable permeability along the migration path of the fault, but also on how the driving pressure compares to the capillary pressure threshold.

The geomodel defined in this study, has a static permeability structure. An additional challenge related to faults, is to include stress-dependency into the properties. Pressure increase due to injection is the main driving force for fluid flow across/along a fault, but it also has the potential to reactivate a fault and further stimulate fluid migration. Permeability changes in the fault are related to failure and slip mechanisms, but less dramatic are the non-linearities in hydro-mechanical properties, due to changes in effective stress, e.g. pore-pressure change. It has been shown that stress-strain behavior in rocks is dominated by the softer parts (Liu, 2017) at low effective stress. What constitutes as low effective stress is relative and material dependent. This soft behavior is manifested in large strain of relatively small features, such as (micro-) fractures and/or other soft components and show an exponential correlation between effective stress and hydraulic properties, such as permeability, porosity and fracture aperture, as well as mechanical properties such as stiffness. Note that a fault zone is usually weaker than the original host rock and has lower failure attributes, such as friction coefficient and cohesion, hence pressure dependency on material properties may be more significant in fault rocks compared to host rocks.

4. Conclusion

Here we address the short-comings of standard geocellular fault models by defining and validating an upscaled multi-layered geocellular description of a fault. The upscaled formulations greatly reduce both the geometrical complexity and computational demand, by collapsing the spatial extent of the fault to a face or a line

with a virtual thickness and, importantly, add the advantage of including slip-surface(s) to the fault.

The upscaled multi-layered geocellular model was validated by comparing the results with a model where the fault was fully-resolved. Cases of 1, 2, 4 and 8 geocellular layers were solved and it was found that, although the upscaled formulation slightly underestimated the flow-rates, the accuracy was found to be high and consistent with generally less than 4 % error (or less than 8 % with 95 % confidence interval). The more layers the more accurate the upscaled model compared to the full-dimensional model. The validation was demonstrated on a 2D model, however, the concept, formulations and methodology are extendable to 3D.

The focus in this work was on validating the model concept and an updated formulation for a multi-layered geocellular fault, but some observations from the validation model were made. Increasing variability in fault composition results in more consistent hydraulic properties, or less spread in results. At the same time, the along-fault flow is relatively stable for various number of geocellular layers (fault variability), while across-fault flow was decreasing with more layers.

Acknowledgements

The work has been performed with support from the project FRISK - Quantification of fault-related leakage risk, under grant number 294719 and the Norwegian CCS Centre, grant number (257579/E20). Many thanks to research partners at NGI, NORCE, UiO and UiB.

References

- [1] Caine, J. S., Evans, J. P., and Forster, C. B. (1996). Fault zone architecture and permeability structure. *Geology*, 24(11):1025-1028.
- [2] Childs, C., Manzocchi, T., Nell, P., Walsh, J., Strand, J., Heath, A., and Lygren, T. (2002). Geological implications of a large pressure difference across a small fault in the Viking Graben. In *Norwegian Petroleum Society Special Publications*, volume 11, pages 187–201. Elsevier.
- [3] Childs, C., Walsh, J. J., Manzocchi, T., Strand, J., Nicol, A., Tomasso, M., Schöpfer, M. P., and Aplin, A. C. (2007). Definition of a fault permeability predictor from outcrop studies of a faulted turbidite sequence, Taranaki, New Zealand. *Geological Society, London, Special Publications*, 292(1):235-258.
- [4] Foxford, K.A., Walsh, J.J., Watterson, J., Garden, I.R., Guscott, S.C. and Burley, S.D., (1998). Structure and content of the Moab Fault Zone, Utah, USA, and its implications for fault seal prediction. *Geological Society, London, Special Publications*, 147(1), pp.87-103.
- [5] Fredman, N., Tveranger, J., Semshaug, S., Braathen, A., and Sverdrup, E. (2007). Sensitivity of fluid flow to fault core architecture and petrophysical properties of fault rocks in siliciclastic reservoirs: a synthetic fault model study. *Petroleum Geoscience*, 13(4):305–320.
- [6] Freeman, S., Harris, S., and Knipe, R. (2008). Fault seal mapping-incorporating geometric and property uncertainty. *Geological Society, London, Special Publications*, 309(1):5-38.
- [7] Grant, N. T. (2020). Stochastic modelling of fault gouge zones: implications for fault seal analysis. *Geological Society, London, Special Publications*, 496(1):163-197.
- [8] Lehner, F. and Pilaar, W. (1997). The emplacement of clay smears in synsedimentary normal faults: inferences from field observations near Frechen, Germany. In Møller-Pedersen, P. and Koestler, A., editors, *Hydrocarbon Seals*, volume 7 of *Norwegian Petroleum Society Special Publications*, pages 39-50. Elsevier.
- [9] Lindsay, N., Murphy, F., Walsh, J., Watterson, J., Flint, S., and Bryant, I. (1993). Outcrop studies of shale smears on fault surfaces. The geological modelling of hydrocarbon reservoirs and outcrop analogues, 15:113-123.
- [10] Liu, H.-H. (2017). Fluid Flow in the Subsurface -History, Generalization and Applications of Physical Laws, volume 28 of *Theory and Applications of Transport in Porous Media*. Springer International Publishing, 1 edition. DOI: 10.1007/978-3-319-43449-0.
- [11] Manzocchi, T., Walsh, J. J., Nell, P., and Yielding, G. (1999). Fault transmissibility multipliers for flow simulation models. *Petroleum Geoscience*, 5(1):53-63.
- [12] Matonti, C., Lamarche, J., Guglielmi, Y., and Mari e, L. (2012). Structural and petrophysical characterization of mixed conduit/seal fault zones in carbonates: Example from the Castellans fault (SE France). *Journal of Structural Geology*, 39:103-121.
- [13] Niemi, A., Bear, J., and Bensabat, J., editors (2017). *Geological Storage of CO₂ in Deep Saline Formations*, volume 29 of *Theory and Applications of Transport in Porous Media*. Springer Netherlands.
- [14] Sperrevik, S., Gillespie, P. A., Fisher, Q. J., Halvorsen, T., and Knipe, R. J. (2002). Empirical estimation of fault rock properties. In Koestler, A. G. and Hunsdale, R., editors, *Hydrocarbon Seal Quantification*, volume 11 of *Norwegian Petroleum Society Special Publications*, pages 109 -125. Elsevier.
- [15] Torabi, A. and Berg, S. S. (2011). Scaling of fault attributes: A review. *Marine and Petroleum Geology*, 28(8):1444-1460.
- [16] Wilson, P., Smith, S., Povey, D., and Harris, S. (2020). Ranking and selecting fault models using flow-indicator fault properties and simple streamline simulations. *Petroleum Geoscience*.
- [17] Wu, L., Thorsen, R., Ottesen, S., Meneguolo, R., Hartvedt, K., Ringrose, P., and Nazarian, B. (2021). Significance of fault seal in assessing CO₂ storage capacity and containment risks - an example from the Horda Platform, northern North Sea. *Petroleum Geoscience*.
- [18] Wu, L., Thorsen, R., Ringrose, P., Ottesen, S., and Hartvedt, K. (2019). Significance of fault seal in assessing CO₂ storage capacity and leakage risks - An example from offshore Norway. In *Fifth International Conference on Fault and Top Seals*, volume 2019, pages 1-5. European Association of Geoscientists & Engineers.
- [19] Yielding, G., Freeman, B., and Needham, D. T. (1997). Quantitative fault seal prediction. *AAPG bulletin*, 81(6):897-917.
- [20] Yielding, G.P.B.S., Bretan, P. and Freeman, B., (2010). Fault seal calibration: a brief review. *Geological Society, London, Special Publications*, 347(1), pp.243-255.